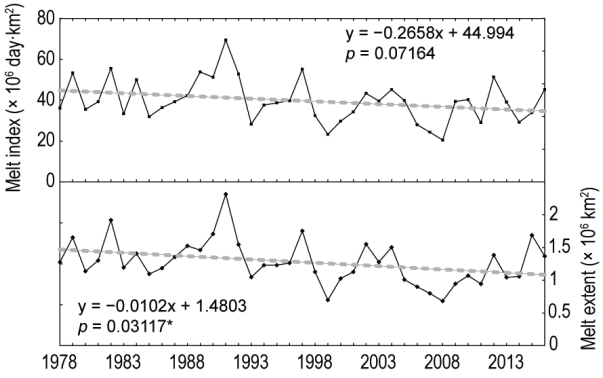

Fig. 6.7. (a) Melt index (× 10^6 day·km^2) from 1978/79 to 2016/17, showing a negative trend (265 800 day·km^2 yr^{-1}, not significant at 95%). (b) Melt extent (× 10^6 km^2) from 1978/79 to 2016/17, showing a negative trend (10 200 km^2 yr^{-1}, $p < 0.05$%). The year on the x-axis corresponds to the start of the austral summer melt season, that is, 2008 corresponds to summer 2008/09.

occurred on the Ross Ice Shelf and small portions of coastal Queen Maud Land. Almost half of the Ross Ice Shelf experienced melt, albeit briefly, in the summer of 2016/17. Compared to the previous year, melt on the Ross Ice Shelf was less extensive. Overall, the 2016/17 melt season was slightly longer than the historical average (Fig. 6.6d), indicating an above-average melt year for Antarctica.

Figure 6.7a shows a non-significant ($p > 0.05$) negative trend (265 800 day·km^2 yr^{-1}) in melt index since 1978, highlighted by the record low melt season observed during austral summer 2008/09. The trend lines were fit using a linear regression between the melt indices and year number. Before adding 2017 to the regression, the negative trend in melt index was significant ($p < 0.05$; Wang and Liu 2017). The marked increase in melt index for 2017 was due to the intensive melt (> 90 days) on the Wilkins Ice Shelf. The negative trend of the melt extent, however, remained significant ($p < 0.05$; Fig. 6.7b), because half of the Ross Ice Shelf did not melt (Fig. 6.6c) as it did in 2016, which reduced the 2017 melt extent as compared to 2016 (Fig. 6.7b). Nonetheless, both the melt extent and melt index were the second highest since 2005. The negative trends are consistent with previous reports (Liu et al. 2006; Tedesco 2009; Tedesco et al.2009).

e. *Sea ice extent, concentration, and seasonality*—P. Reid, S. Stammerjohn, R. A. Massom, J. L. Lieser, S. Barreira, and T. Scambos

Antarctic sea ice performs important roles in the climate system through the formation of dense oxygen rich Antarctic Bottom Water (Johnson 2008) and modulating fluxes across the ocean/atmosphere interface within the high southern latitudes (Bourassa et al. 2013). It also acts as a buffer for ice shelves against ocean processes (Williams and Squire 2007; Massom et al. 2018).

Net sea ice extent (SIE; the area enclosed by the ice edge consisting of a range in sea ice concentration) and sea ice area (SIA; the actual area covered by sea ice) were well below the 1981–2010 average for all of 2017 (Fig. 6.8b). Following the record low seasonal sea ice cover in November and December 2016 (Reid et al. 2017; Stuecker et al. 2017; Turner et al. 2017; Schlosser et al. 2018), the first four months of 2017 also had record low net SIE, followed by sporadic periods of record low SIE into September. Overall, 130 days of record low SIE occurred during 2017, with 57 individual days of record low SIA between January and early October. The month of February 2017 recorded the lowest monthly mean SIE on record (Schlosser et al. 2018). Other records in 2017 included the lowest observed daily value of SIE in the continuous satellite record (since 1978) on 1 March 2017 of 2.1×10^6 km^2 (not shown; previous lowest was 2.3×10^6 km^2 on 27 February 1997). The annual daily maximum was also later than previously observed, on 9 October (previous latest maximum was 3 October 1988). Record low sea ice cover during 2016/17 is in contrast to the long-term (1979–2016) positive trend in net SIE (Turner and Comiso 2017), as discussed further below.

Regionally, early 2017 (January through mid-April) sea ice coverage followed on from the predominantly low net sea ice coverage in late 2016. However, high concentrations of sea ice were observed along much of the coast of East Antarctica (~80°–160°E) and in parts of the Weddell Sea (~30°–60°W), for example (Fig. 6.8c). Synoptically, in late 2016 and January 2017, winds around East Antarctica and the Weddell Sea were anomalously easterly, causing an initial southward compaction of the sea ice via Ekman transport while largely retaining the sea ice extent in these regions during the summer season (Figs. 6.8a,c). Consequently, sea ice advanced early across much of East Antarctica. Elsewhere around the coast in early 2017, sea ice coverage was either non-existent or well below average (e.g., Fig. 6.8c). Ocean SSTs around Antarctica through early 2017 were anomalously high (e.g., Fig. 6.8c; Section 6f) and coincident with regions of suppressed ice formation, particularly in the Ross, Bellingshausen, and Amundsen Seas and the eastern Weddell Sea. The suppressed ice formation led to considerably later ice edge advance in these regions, by as much as 50 days later in most of the Amundsen

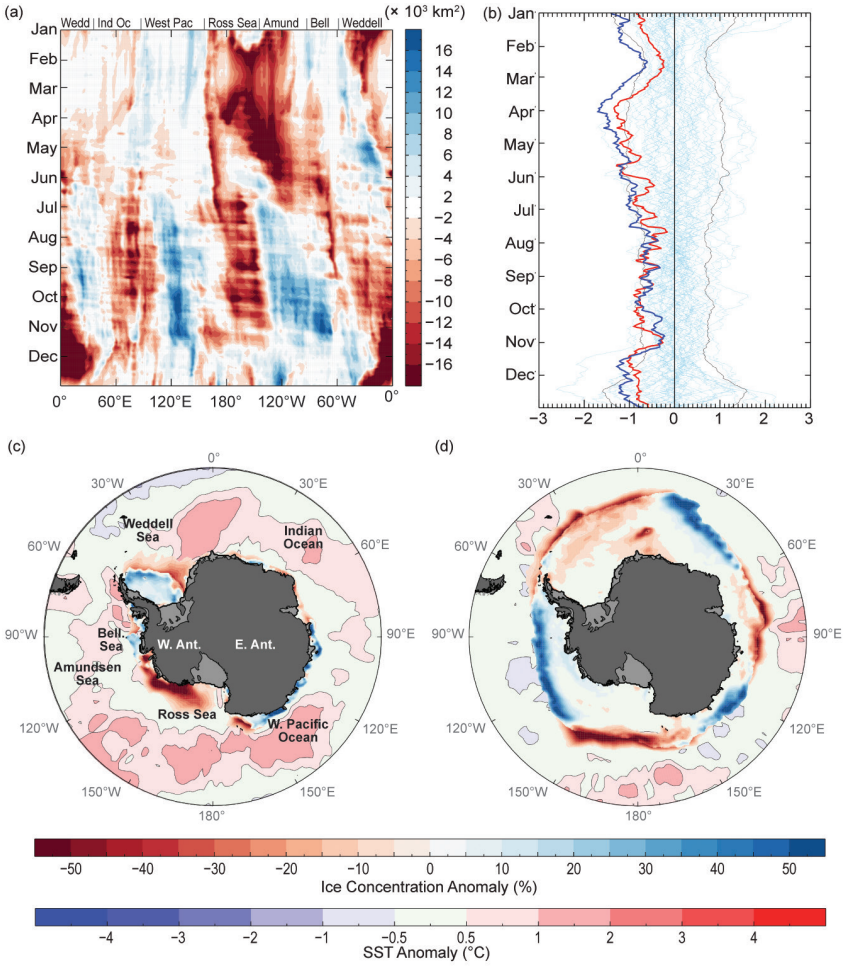

Fig. 6.8. (a) Hovmöller plot of daily SH sea ice extent anomalies for 2017 (× 10³ km² per degree of longitude; from the 1981–2010 mean); (b) net sea ice extent anomaly (blue) and sea ice area anomaly (red) (from 1981–2010 mean); thin blue lines represent the historical daily values of extent for 1979–2015, while the thin black lines represents ±2 std. dev. of extent. (c) and (d) sea ice concentration anomaly (%) and SST anomaly (°C; Reynolds et al. 2002; Smith et al. 2008) for (c) Feb. and (d) Sep. 2017. Based on satellite passive-microwave ice concentration data [Cavalieri et al. 1996, updated yearly, for climatology; and Maslanik and Stroeve (1999) for the 2017 sea ice concentrations].

Sea, as reflected in the negative duration anomaly in this region (Fig. 6.9a).

The atmospheric circulation pattern changed during April with deep low pressure systems developing north of the Weddell Sea (~30°W), Wilkes Land (~125°E), and well north of the Amundsen Sea (~100°W; see Section 6b). This pattern enhanced ice coverage predominantly within the western Weddell Sea while continuing to suppress extent in the Bellingshausen, Amundsen, and Ross Seas through warm air advection and higher-than-normal SSTs. A zonal wave-two atmospheric pattern developed in May (not shown), with synoptic lows centered in the eastern Ross Sea (~140°W) and north of the Amery Ice Shelf (~70°E), promoting sea ice advance (albeit later than normal) in the Ross (~120°W–180°) and Weddell (~10°–30°W) Seas. Through May and into early June, SIE continued to be above average across much of East Antarctica but below average in the western Ross, Amundsen, and Bellingshausen Seas and across the eastern Weddell Sea and Indian Ocean sectors (~10°W–80°E).

During mid-June, a stationary wave-three atmospheric pattern began to develop (Section 6b), with broad low-pressure centers to the north of the Bellingshausen Sea (~80°W), East Antarctica (~140°E), and Dronning Maud Land (~40°E) that broadly correspond to the SIE anomalies (Fig. 6.8a). This pattern increased southerly cold air outflow in the eastern Ross Sea, far eastern Weddell Sea, and north of Wilkes Land (~120°E), increasing ice coverage and contributing to a positive anomaly in SIE in these regions (Fig. 6.8a). Conversely, intervening warm air advection and higher SSTs associated with this zonal wave-three pattern were observed in the western Weddell and Ross Seas and to the north of the Amery Ice Shelf (~60°–100°E), suppressing ice expansion and producing a negative SIE anomaly (Fig. 6.8a). Interestingly, while the atmospheric zonal wave-three pattern subsided during September, the zonal wave-three pattern within both the patterns of SIE and SST anomalies persisted through early November (Figs. 6.8a,d). It was during this period (September onwards; e.g., Fig. 6.8d) that, again similar to 2016 (Mazloff et al. 2017; Reid et al. 2017), the Maud Rise polynya opened up (see Sidebar 6.1).

Early November saw another change in the circumpolar atmospheric circulation pattern, with the development of a deep Amundsen Sea low pressure system and an associated zonal wave-three pattern. The change in atmospheric circulation influenced

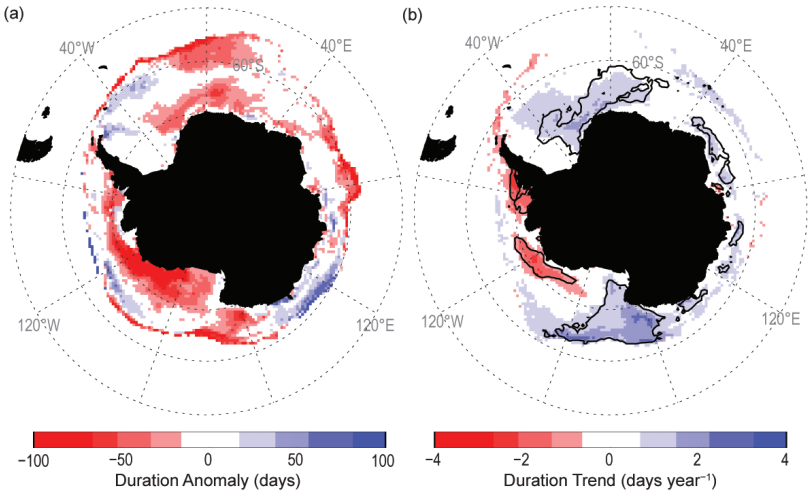

Fig. 6.9. Maps showing (a) duration anomaly for the 2016/17 sea ice season in days and (b) duration trend for 1979/80–2016/17 in days yr^{-1}. The black contour in (b) delineates those trends with significance at the $p < 0.01$ significance level.

the regional rate of ice retreat, particularly in the Bellingshausen–Amundsen (60°–120°W) and Weddell (30°W–30°E) Seas where slower and faster retreat occurred, respectively (Fig. 6.8a).

These austral springtime sea ice distribution changes are consistent with the influence of the relatively weak La Niña developing within the tropical Pacific in early November 2017 (see Section 4b), which changed the position of the higher-latitude southern jet streams and hence the cyclonicity around the Antarctic continental edge (Yuan 2004; Stammerjohn et al. 2008). Thus, SIE towards the end of the year and within the Weddell Sea was, in some areas, more than six standard deviations below average. Elsewhere, SIE was close to average, although small pockets of greater-than-average SIE existed within the Amundsen Sea and western Pacific sector (~110°–150°E) associated with wind-driven compaction of the sea ice cover and lower-than-normal SSTs near these regions.

The long-term trend for Antarctic sea ice is regionally and seasonally variable: increased SIE and longer seasonal duration within the Ross and Weddell Seas, and decreased SIE and shorter duration in the Bellingshausen–Amundsen Seas (e.g., Fig. 6.9b for sea ice duration trends over 1979/80–2016/17; see Comiso et al. 2017 for sea ice extent trends). For SIE these changes are largest during January–May (Hobbs et al. 2016). Apart from some areas of the Amundsen Sea, the regional pattern of sea ice coverage during 2017, described above, was in contrast to this long-term trend (Fig. 6.9a), particularly in much of the Ross Sea and the Weddell Sea through the end of March.

f. Southern Ocean—S. Swart, K. Johnson, M. R. Mazloff, A. Meijers, M. P. Meredith, L. Newman, and J.-B. Sallée

In the climate system, the Southern Ocean is disproportionately important when it comes to its storage of heat and carbon. Modification of the upper Southern Ocean could have significant implications for the rate and magnitude of air–sea fluxes (of heat and carbon) and for the ventilation of the ocean interior, thereby altering the effects of climate warming on the ocean system as a whole. Here, we evaluate the state of the Southern Ocean in 2017 by first assessing the upper ocean as the interface between the atmosphere and ocean interior. We then discuss the changes in intermediate to deep water masses, which are critical pathways to moving heat and carbon to the ocean interior where it will (in general) remain for decades to centuries. Lastly, we report on the status of ocean acidification in the Southern Ocean using newly available biogeochemical observations.

1) Upper ocean

By utilizing all available 2017 hydrographic profiles (40 816 from Argo floats and 11 916 from tagged seals), anomalies of mixed layer depth (MLD) and mixed layer (ML) temperature and salinity (Figs. 6.10a–c) were computed from the climatological (2000–2010) seasonal cycle (see Pellichero et al. 2017). During 2017, the most significant observation is the shallower MLDs (negative anomalies) occurring in the Pacific sector, particularly within the Antarctic Circumpolar Current (ACC), where MLDs are more than 100 m shallower than the climatology. Meanwhile, the Atlantic and Indian sectors are characterized by mixed MLD anomalies.

In contrast to anomalies reported for 2015 and 2016 (Sallée et al. 2016; Mazloff et al. 2017), a markedly warmer ML (Fig. 6.10b) was observed throughout most of the Southern Ocean in 2017, except for the northern subantarctic region of the Atlantic sector. In further contrast, positive Southern Ocean ML temperature anomalies in 2015 were juxtaposed against negative anomalies to the north, indicating a north–south dipole separated by the ACC (Sallée et al. 2016), while in